Received: 15 June 2023 | Accepted: 30 October 2023

DOI: 10.1111/bpa.13222

RESEARCH ARTICLE

Brain Pathology

Structural changes of CA1 pyramidal neurons after stroke in the contralesional hippocampus

Paula Merino-Serrais[1,2] | **Sergio Plaza-Alonso**[1,2] | **Farida Hellal**[3,4,5] | **Susana Valero-Freitag**[3] | **Asta Kastanauskaite**[1,2] | **Nikolaus Plesnila**[3,5] | **Javier DeFelipe**[1,2,6]

[1]Laboratorio Cajal de Circuitos Corticales, Centro de Tecnología Biomédica, Universidad Politécnica de Madrid, Madrid, Spain

[2]Departamento de Neurobiología Funcional y de Sistemas, Instituto Cajal, CSIC, Madrid, Spain

[3]Laboratory of Experimental Stroke Research, Institute for Stroke and Dementia Research (ISD), University Hospital, Ludwig-Maximilians-University Munich (LMU), Munich, Germany

[4]iTERM, Helmholtz Center, Munich, Germany

[5]Munich Cluster of Systems Neurology (Synergy), Munich, Germany

[6]CIBER de Enfermedades Neurodegenerativas, Instituto de Salud Carlos III, Madrid, Spain

Correspondence
Paula Merino-Serrais, Departamento de Neurobiología Funcional y de Sistemas, Instituto Cajal (CSIC), Avenida Doctor Arce, 37, 28002 Madrid, Spain.
Email: paula.merino-serrais@cajal.csic.es

Funding information
Centro de Investigación Biomédica en Red sobre Enfermedades Neurodegenerativas, Grant/Award Number: CB06/05/0066; Deutsche Forschungsgemeinschaft, Grant/Award Number: 390857198; ERA-NET NEURON, Grant/Award Number: PCI2018-092874; MCIN/AEI/10.13039/501100011033, Grant/Award Numbers: IJCI-2016-27658, PID2021-127924NB-I00; Spanish Ministry of Universities, Grant/Award Number: FPU19/00007

Abstract

Significant progress has been made with regard to understanding how the adult brain responds after a stroke. However, a large number of patients continue to suffer lifelong disabilities without adequate treatment. In the present study, we have analyzed possible microanatomical alterations in the contralesional hippocampus from the ischemic stroke mouse model tMCAo 12–14 weeks after transient middle cerebral artery occlusion. After individually injecting Lucifer yellow into pyramidal neurons from the CA1 field of the hippocampus, we performed a detailed three-dimensional analysis of the neuronal complexity, dendritic spine density, and morphology. We found that, in both apical (*stratum radiatum*) and basal (*stratum oriens*) arbors, CA1 pyramidal neurons in the contralesional hippocampus of tMCAo mice have a significantly higher neuronal complexity, as well as reduced spine density and alterations in spine volume and spine length. Our results show that when the ipsilateral hippocampus is dramatically damaged, the contralesional hippocampus exhibits several statistically significant selective alterations. However, these alterations are not as significant as expected, which may help to explain the recovery of hippocampal function after stroke. Further anatomical and physiological studies are necessary to better understand the modifications in the "intact" contralesional lesioned brain regions, which are probably fundamental to recover functions after stroke.

KEYWORDS
contralesonal hemisphere, dendritic spines, intracellular injections, neuronal complexity, tMCAo

1 | INTRODUCTION

Stroke is one of the major causes of death and disability worldwide [1]. After stroke, the quality of life of the patients is often deficient, with constant care needed for the rest of the individual's life. Moreover, stroke is considered a high-risk factor for cognitive impairment and dementia [2–4]. In stroke research, numerous studies suggest that the failure of performance in multiple regions of the brain after a stroke could be explained by the so called Monakow's theory of diaschisis. This theory describes neurophysiological alterations in areas that are

distant from a focal brain lesion, including changes in blood flow, metabolism, atrophy, and alterations in glucose metabolism [5–8]. Accordingly, this concept could explain how after stroke, remote regions anatomically connected to the infarcted area are also affected and therefore influence neuronal functional recovery [9–11]. Thus, diaschisis in the contralesional hemisphere could be explained by deafferentation, defined as a loss of neuronal input from the damaged area [12].

However, despite the enormous clinical and preclinical advances in understanding the acute and life-threatening consequences of stroke in recent decades, new and more effective therapeutic approaches are clearly required.

In humans, numerous brain regions may be exposed to ischemic stroke, depending on the location of the lesion, including the hippocampal formation. This region, together with the perirhinal area and the posterior parahippocampus, constitutes the mesial memory system, which plays a crucial role in the processing and consolidation of memory. Accordingly, in the present study we have focused on the possible alterations of the principal cells in the contralesional hippocampus, namely the pyramidal neurons. The hippocampal formation is a structure of bidirectional information flow from all cortical associative regions of the central nervous system [13, 14], and it has been demonstrated that it is involved in the consolidation of both semantic and episodic declarative memory. In addition, it participates in the elaboration of visuospatial memory, which involves the memory of spatial configurations [13, 15].

The CA1 field of the hippocampus is one of the most extensively studied regions of the cerebral cortex. This hippocampal field receives and integrates a massive amount of information, playing an essential role in the functioning of the proper hippocampal circuitry [16]. Moreover, it has been suggested that memory-related hippocampal dysfunction may be due to structural and functional alterations in the hippocampus and/or in neocortical regions linked to working memory functions [17–19].

The main apical, collateral, and basal dendrites of pyramidal cells are considered to be synaptic input units, set up as different cellular compartments, which receive and integrate different presynaptic excitatory and inhibitory inputs, acquiring particular connection and functional characteristics [20–23]. The morphology and complexity of the different cellular compartments influence the biophysical and computational properties of the neurons, and the formation of the synaptic connections then modulates cortical circuitry [24–29].

Another fundamental characteristic of pyramidal cells is that their dendrites are covered with dendritic spines (for simplicity, spines). Spines are generally considered as plastic structures crucial to memory, learning, and cognition, whose formation and elimination have been linked to memory storage capacity [30–33].

Spines are the major postsynaptic elements of excitatory glutamatergic synapses [33–35], and alterations in spine density and morphology influence the cortical circuitry, and therefore affects proper brain function [36–39]. Moreover, it is widely assumed that the stability of spines and dendrite arbors is crucial for the proper functioning of the adult brain, and possible alterations could be associated with common neurological disorders including stroke [40]. Several studies have shown that specific treatments and rehabilitation training could modulate the neuronal complexity and synaptic activity after stroke in the cerebral cortex, including the hippocampus [41–43].

Importantly, it has been demonstrated that pyramidal neurons are more susceptible to ischemic stroke than other neuronal types [44] and that the preservation of pyramidal cells may represent an important plastic potential after stroke [45]. Therefore, the study of possible microanatomical changes in CA1 pyramidal neurons in the contralesional hippocampus after experimentally induced ischemic stroke serves as an excellent opportunity to advance in the knowledge of diaschisis to better explain brain dysfunction after stroke in a distant brain region.

Using the same experimental stroke model, we have previously reported that in the contralesional somatosensory cortex (SSCx), pyramidal neurons from layer III showed selective morphological alterations in the complexity of the dendritic arbor and spine morphology [46]. In the present study, we have analyzed whether dendritic complexity, spine density, and morphology are impaired in CA1 pyramidal neurons from the contralesional hippocampus after stroke, using intracellular injections of Lucifer yellow (LY) to reconstruct single CA1 pyramidal neurons.

Our results show that ischemic stroke induces a significantly higher complexity and reduction in spine density as well as changes in spine morphology in both apical and basal arbors, in the contralesional CA1 pyramidal neurons. Our findings also suggest that these changes differ from those observed in pyramidal neurons of the SSCx.

2 | MATERIALS AND METHODS

2.1 | tMCAo model

Experiments were performed on adult male C57BL/6N mice (12–16 weeks old; body weight, 23–26 g; Charles Rivers Laboratories). All experimental procedures were conducted in accordance with European regulations, the ethical committee of Upper Bavaria (Vet 2-15-196) and in compliance with the ARRIVE (Animal Research: Reporting In Vivo Experiments) criteria [47].

Transient middle cerebral artery occlusion (tMCAo) was performed on the left middle cerebral artery. Then, reperfusion was induced by withdrawal of the filament after 1 h of occlusion, as previously described elsewhere [48]. The occlusion was confirmed by decreased regional cerebral blood flow (CBF) monitored by a laser Doppler probe fixed to the skull above the tMCAo territory and a pulse oximeter monitored the vital parameters. Sham-operated mice underwent the same surgery without occlusion of the MCA and

received the same post-operative care (see Reference [46] for further details).

2.2 | Intracellular injections, confocal microscopy acquisition and 3D microanatomical reconstruction in CA1 pyramidal neurons

For LY intracellular injections, 12–14 weeks after tMCAo induction, the animals were anesthetized by intraperitoneal injection of midazolam (5 mg/kg; Braun, Melsungen, Germany), fentanyl (0.05 mg/kg; Janssen-Cilag, Neuss, Germany), and medetomidine (0.5 mg/kg; Pfizer, Karlsruhe, Germany), and then intracardially perfused with phosphate buffer pH 7.4 (PB) followed by 4% paraformaldehyde (PFA). The brains were then postfixed in PFA for 24 h. Coronal sections (150 μm-thick, 2–4 sections per animal) were obtained on a vibratome and were then prelabeled with 4,6 diamino-2-phenylindole (DAPI; Sigma, St Louis, MO) to visualize the nuclei. LY (LY; 8% in 0.1 M Tris buffer, pH 7.4) was applied by continuous current to each individual CA1 pyramidal cell until the individual dendrites of the cell could be traced to an abrupt end at their distal tips (that fluoresced brightly) and their spines were readily visible. In addition, the fluorescence did not diminish at a distance from the soma, indicating that the dendrites were completely filled [49]. Finally, the sections were mounted in glycerol (50% in 0.1 M PB, 0.1% azide) and analyzed using confocal microscopy. In addition, adjacent sections (50 μm either side of the 150 μm-thick sections) were Nissl-stained to identify the cortical and subcortical areas and the extent of the ischemic lesson (Figure 1).

As previously described in [46], for three-dimensional (3D) neuronal reconstruction, pyramidal neurons from CA1 pyramidal layer were recorded by confocal microscopy with a ZEN inverted scanning confocal system (Zeiss LSM 710; Carl Zeiss Microscopy GmbH, Jena, Germany) using a 488 nm Argon laser and 405 nm UV and the fluorescence of DAPI and Alexa 488 were recorded through separate channels. The image stacks were recorded at 0.45 μm intervals with a 40× oil-immersion lens (NA, 1.3, refraction index, 1.51) and 0.9 zoom (image resolution: 1024 × 1024 pixels; pixel size: 0.23 μm). No pixels were saturated within the spines. Before the analysis, all image stacks for stroke and sham conditions were coded and the morphological analyses were performed blindly. Finally, 439 single pyramidal neurons from the CA1 region were individually injected with LY (190 in sham-operated and 249 in tMCAo mice; 4–20 neurons per section).

Subsequently, the labeled pyramidal neurons were 3D reconstructed by tracing the neuronal structure, including 30 individual apical and 30 basal dendritic arbors per group ($n = 4$–6 mice per group). Confocal images containing the dendritic arbors, from both apical and basal dendritic trees, were traced using the Neurolucida 360 software (MicroBrightField Inc., Williston, VT). Then, the reconstructed neuronal structures were exported to Neurolucida Explorer (MicroBrightField Inc., Williston, VT) to perform the quantitative analysis.

Dendritic arbor complexity for apical (*stratum radiatum*) and basal (*stratum oriens*) arbors was assessed by measuring several morphological parameters including dendritic length, dendritic volume, number of intersections, dendritic surface area, and dendritic diameter as a function of the distance from the soma, creating concentric spheres—centered on the cell body—of increasing 10-μm radii (Sholl analysis). In addition, dendritic length, dendritic volume, dendritic surface area, and dendritic diameter were measured per branch order (1, 2, and 3). Branch order analysis calculates each morphological parameter based on different dendritic segments derived from dendrite branching. Only dendritic segments that were completely reconstructed were included in the analysis. For apical arbors, main apical dendrites and collateral dendrites were analyzed individually [50].

Furthermore, spine density and spine morphology analyses ($n = 3$–4 mice per group) were conducted on apical collateral dendrites (*stratum radiatum*; 15–17 dendrites per group) and basal dendrites (*stratum oriens*; 20 dendrites per group) using Neurolucida 360 software. Only dendrites that were completely reconstructed were included in the analysis. For spine analysis, the spines were marked by tracing all protrusions considered as spines, applying no correction factors to the spine counts. The reconstructed dendrites were then exported to Neurolucida Explorer to perform the quantitative analysis for spine density and spine morphology. Spine density was calculated for each dendrite by dividing the number of spines by the dendritic length. Furthermore, spine density, spine volume, and spine length per dendrite were measured as a function of the distance from the soma for basal dendrites and from the apical trunk to apical collateral dendrites (Sholl analysis).

Unfortunately, the spine density and spine morphology in the main apical trunks, could not be analyzed due to technical issues.

2.3 | Statistical analysis

All the statistical analyses were performed using the GraphPad Prism 9 and R (4.1.2) software. To compare the averages, unpaired Mann–Whitney test was used to test the overall effect. Values as a function of the distance from the soma were compared using Two-way ANOVA repeated measures (Sholl analysis; p and F values + interaction; degrees of freedom, d.f.). To analyze whether the spine volume and spine length were influenced by the dendritic length, ANCOVA test was performed ($Pr > F$ condition * dendritic length). Data values are expressed as mean ± SEM. In all cases, $p < 0.05$ and $Pr < 0.05$ were considered to be significant (* < 0.05, ** < 0.01, and *** < 0.001).

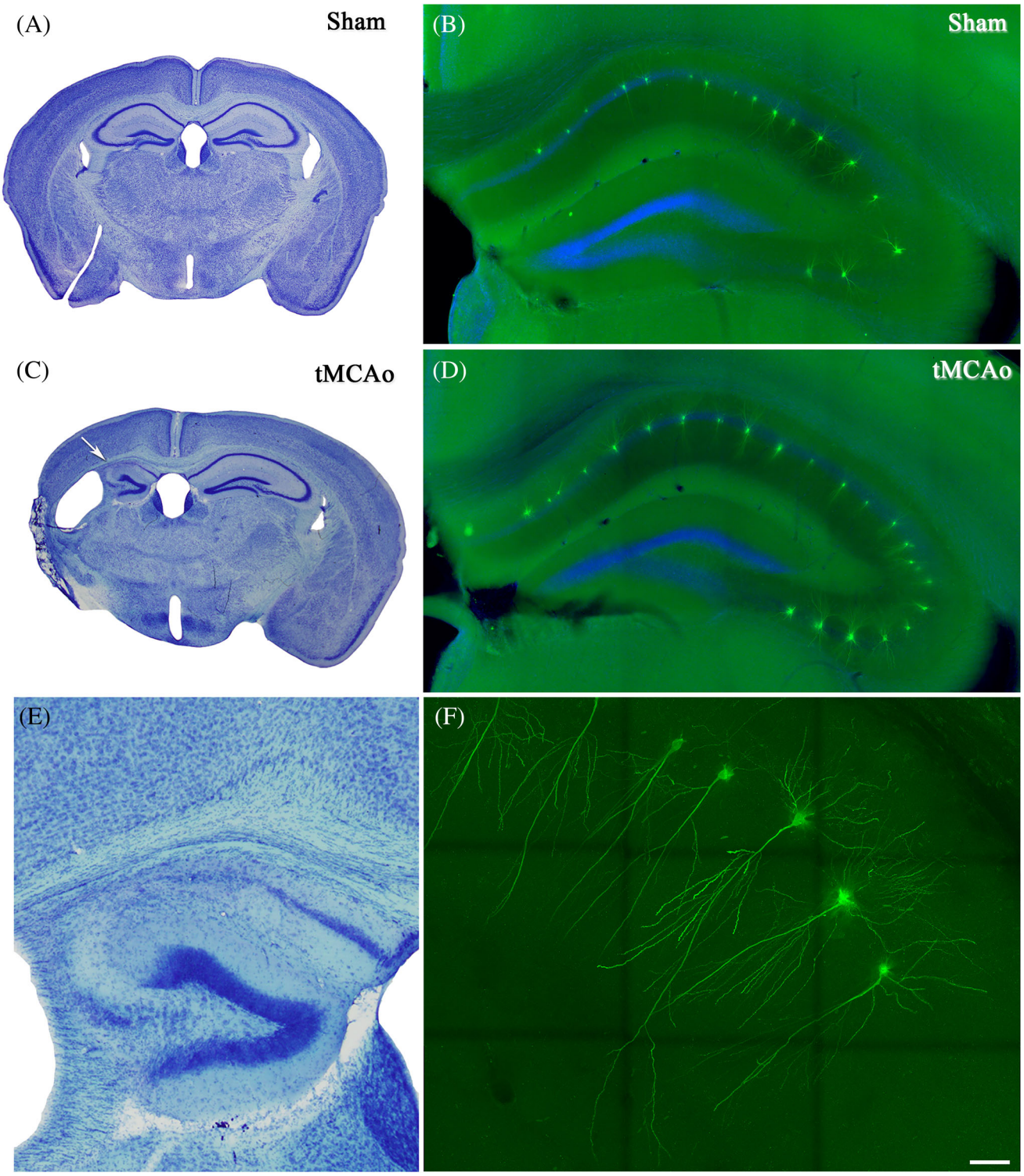

FIGURE 1 Hippocampal ischemic lesion and LY-intracellular injections in the contralesional CA1 pyramidal cell layer. (A,C) Panoramic images of coronal sections stained with Nissl from sham-operated (A) and tMCAo (C) mice showing the ischemic lesion in the left hemisphere. Note the extended atrophy of the hippocampus in the left hemisphere (arrow). (E) Higher magnification of the hippocampal region indicated with an arrow in C. (B,D) Confocal images showing CA1 hippocampal pyramidal neurons individually injected with LY in sham-operated (C) and tMCAo (D) mice. (F) Confocal microscopy image of single LY-injected pyramidal neurons in the CA1 region from a sham-operated animal. Scale bar in F indicates 1 mm in A, C; 300 μm in B, D; 150 μm in E and 50 μm in F.

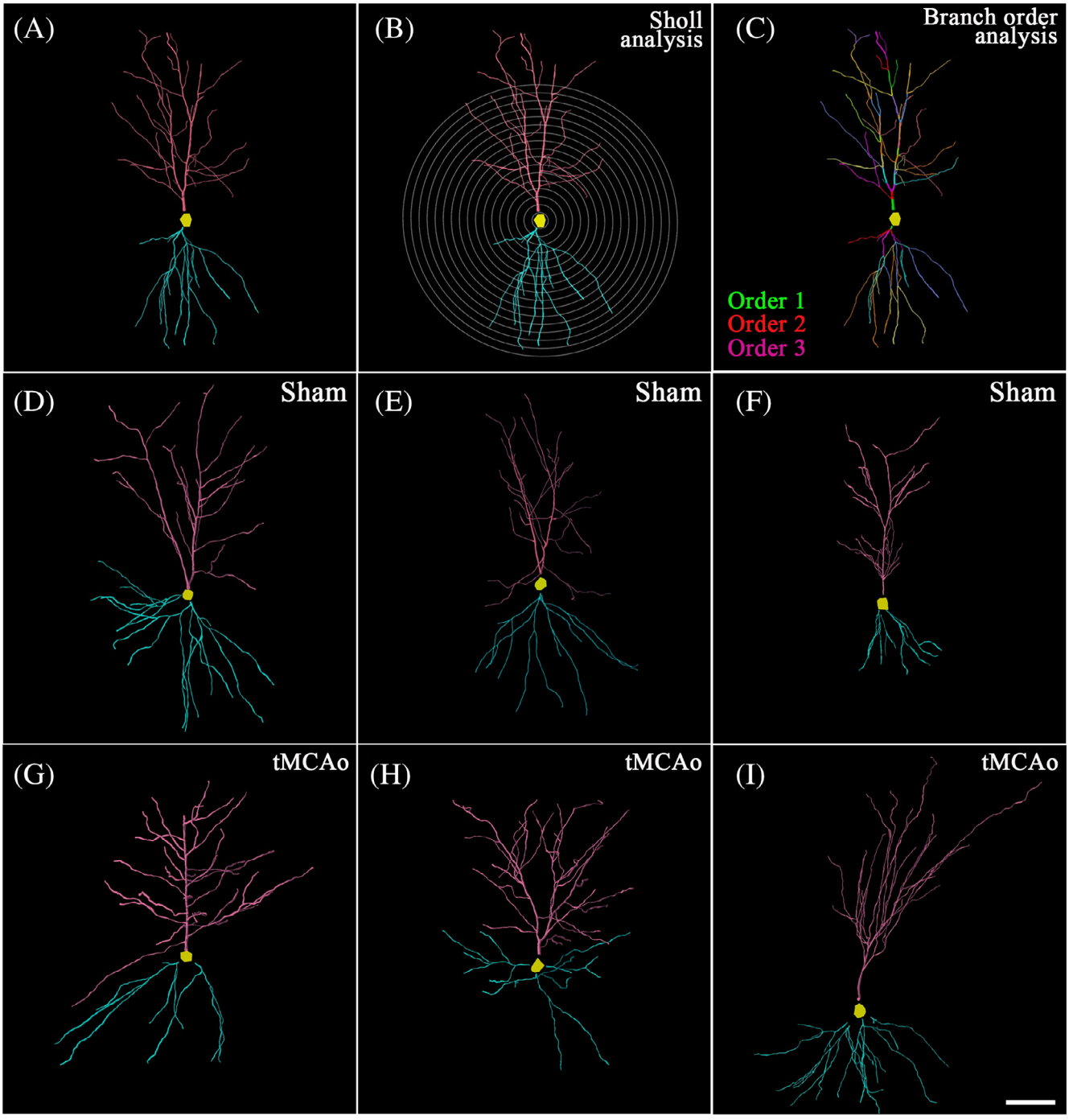

FIGURE 2 LY-injected pyramidal neurons and neuronal reconstruction. (A) Neuronal reconstruction from a sham-operated animal analyzed with Neurolucida software, showing the Sholl analysis (B) and the branch order analysis (C). (D–F) Examples of neuronal reconstructions from sham-operated animals. (G–I) Examples of neuronal reconstructions from tMCAo animals. In all the neuronal reconstructions, the basal dendritic arbor is indicated in cyan and the apical dendritic arbor in pink. Scale bar shown in I indicates 60 μm.

3 | RESULTS

To study whether ischemic stroke could induce microanatomical alterations in CA1 pyramidal neurons from the contralesional hippocampus, we performed an extensive morphometric analysis in the tMCAo model 12–14 weeks after tMCAo (Figure 1). First, we examined the complexity of both apical (*stratum radiatum*) and basal (*stratum oriens*) dendritic arbors and then the spine density and morphology.

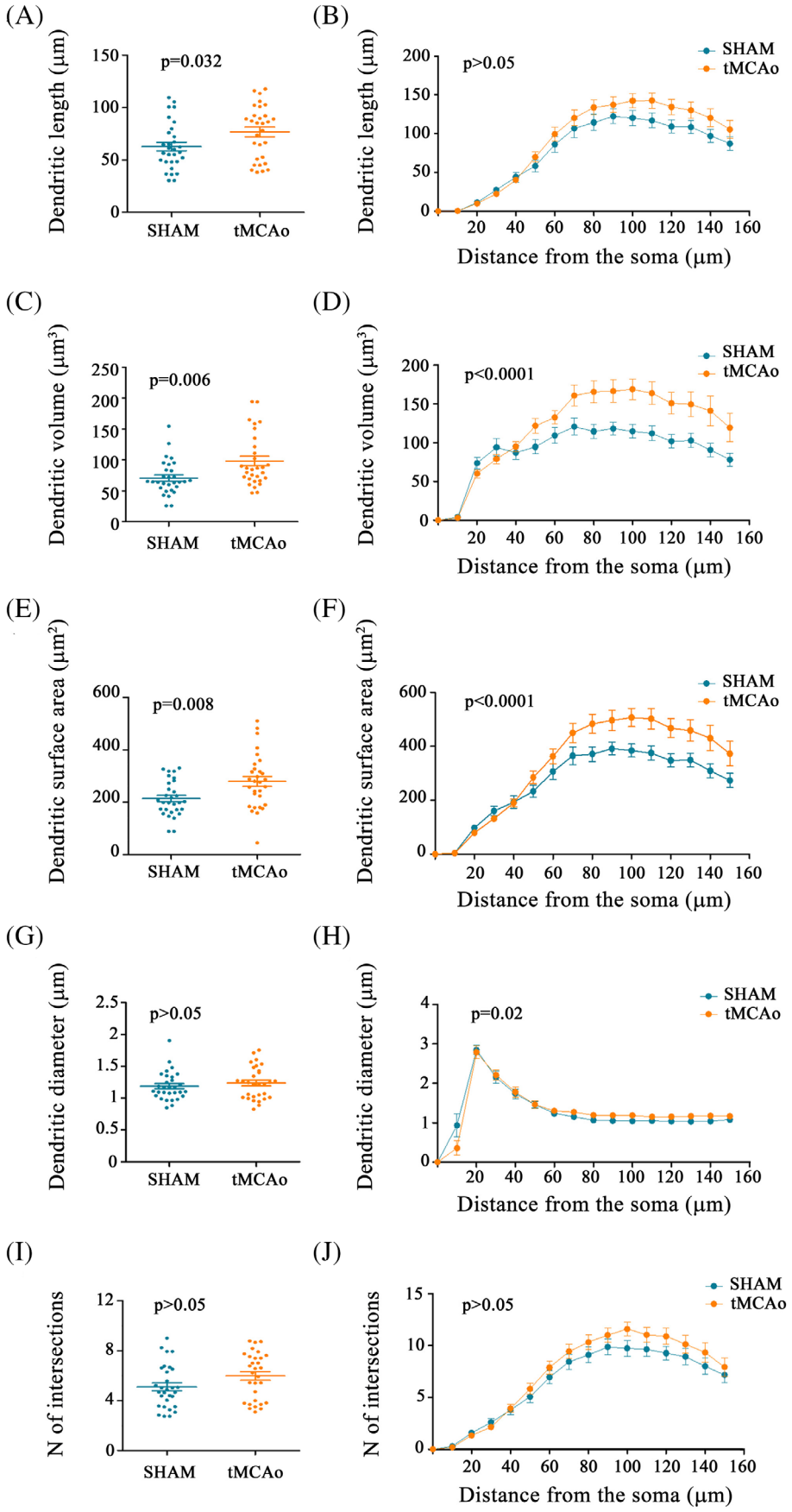

FIGURE 3 Analysis of the complexity of apical dendritic arbors. Comparative morphometric analysis (30 individual apical branches per group) between sham-operated and tMCAo mice ($n = 4$–6 mice per group) of (A,B) dendritic length, (C,D) dendritic volume, (E,F) dendritic surface area, (G,H) dendritic diameter and (I,J) number of intersections, as the average (A,C,E,G,I; unpaired Mann–Whitney test) and as a function of the distance from the soma (B,D,F,H,J; Two-way ANOVA repeated measures).

TABLE 1 Morphological analysis data for apical and basal dendritic arbors.

		Dendritic length (μm)		Dendritic volume (μm^3)		Dendritic surface area (μm^2)		Dendritic diameter (μm)		No. of intersections	
		Sham	tMCAo	Sham	tMCAo	Sham	tMCAo	Sham	tMCAo	Sham	tMCAo
Apical dendritic arbor	Mean ± SEM	62.83 ± 4.08	76.81 ± 4.64	70.82 ± 5.06	98.09 ± 7.74	214.4 ± 12.31	279.8 ± 18.95	1.18 ± 0.04	1.23 ± 0.04	5.1 ± 0.31	5.98 ± 0.34
	Unpaired Mann–Whitney	*p = 0.03*		*p = 0.006*		*p = 0.008*		$p > 0.05$		$p > 0.05$	
	Two-ay ANOVA	$p > 0.05$; $F = 1.5$, d.f. = 14		*p < 0.0001*; $F = 5.44$, d.f. = 14		*p < 0.0001*; $F = 4.04$, d.f. = 14		$p = 0.02$; $F = 1.92$, d.f. = 14		$p > 0.05$; $F = 1.19$, d.f. = 14	
Basal dendritic arbor	Mean ± SEM	60.98 ± 3.98	69.02 ± 4.78	47.72 ± 4.91	59.61 ± 7.42	181.2 ± 13.47	214.5 ± 19.23	0.88 ± 0.03	0.92 ± 0.03	5.34 ± 0.36	6.01 ± 0.4
	Unpaired Mann–Whitney	$p > 0.05$		$p > 0.05$		$p > 0.05$		$p > 0.05$		$p > 0.05$	
	Two-way ANOVA	*p = 0.01*; $F = 2.32$, d.f. = 9		$p > 0.05$; $F = 1.42$, d.f. = 9		$p = 0.03$; $F = 2.07$, d.f. = 9		$p > 0.05$; $F = 0.33$, d.f. = 9		*p = 0.001*; $F = 3.04$, d.f. = 9	

3.1 | Pyramidal apical dendritic arbors of the contralesional CA1 field show higher neuronal complexity

To study whether the dendritic structure of the pyramidal neurons in the contralesional CA1 region is affected after stroke, we performed a detailed morphometric analysis (Figure 2). Neuronal complexity of the apical dendritic arborization was analyzed by measuring the following morphometric parameters: dendritic length, dendritic volume, dendritic surface area, dendritic diameter, and number of intersections. Additionally, a Sholl analysis was performed [51] to discern possible differences for the morphometric parameters as a function of the distance from the soma (Figure 3). Apical dendritic arborization includes both main apical and apical collateral dendrites (*stratum radiatum*).

Significant differences were found in tMCAo compared with sham-operated mice in one or both of the statistical analyses carried out for each morphological parameter studied (see Table 1): tMCAo mice showed higher dendritic length (Figure 3A,B), dendritic volume (Figure 3C,D), dendritic surface area (Figure 3E,F), and dendritic diameter (Figure 3G,H).

However, no significant differences were found in tMCAo mice regarding the number of intersections (Figure 3I,J) compared with sham-operated mice.

In addition, to study if the significant differences found previously were specific to the different neuronal compartments, we performed a further morphological analysis (Figure 4). Specifically, several morphometric parameters were measured per branch order (1, 2, and 3) in the dendritic segments that were completely reconstructed. The main apical dendrite and collateral branches (*stratum radiatum*) were analyzed separately for apical arbors. The main apical dendritic volume was statistically different in tMCAo compared with sham-operated mice for the order 1 and 3 dendritic segments (unpaired Mann–Whitney, $p = 0.003$, both; Figure 4B). Similarly, branch order 1 showed a higher main apical dendritic surface area in tMCAo mice (unpaired Mann–Whitney, $p = 0.039$; Figure 4C). No statistical differences were found for main apical dendritic length or main apical dendritic diameter (unpaired Mann–Whitney, $p > 0.05$; Figure 4A,D, respectively).

Regarding the analysis of collateral dendrites, the dendritic volume was statistically larger in tMCAo mice than in sham-operated mice in the case of the order 1 and 3 dendritic segments (unpaired Mann–Whitney, $p = 0.003$, both; Figure 4F). Similarly, branch order 1 showed a higher dendritic surface area in tMCAo mice (unpaired Mann–Whitney, $p = 0.039$; Figure 4G). The collateral dendritic diameter in tMCAo mice showed significantly higher values for branch order 1, 2, and 3 (unpaired Mann–Whitney, $p = 0.0001$; $p = 0.008$; and $p < 0.0001$, respectively; Figure 4H). No statistical differences were found for

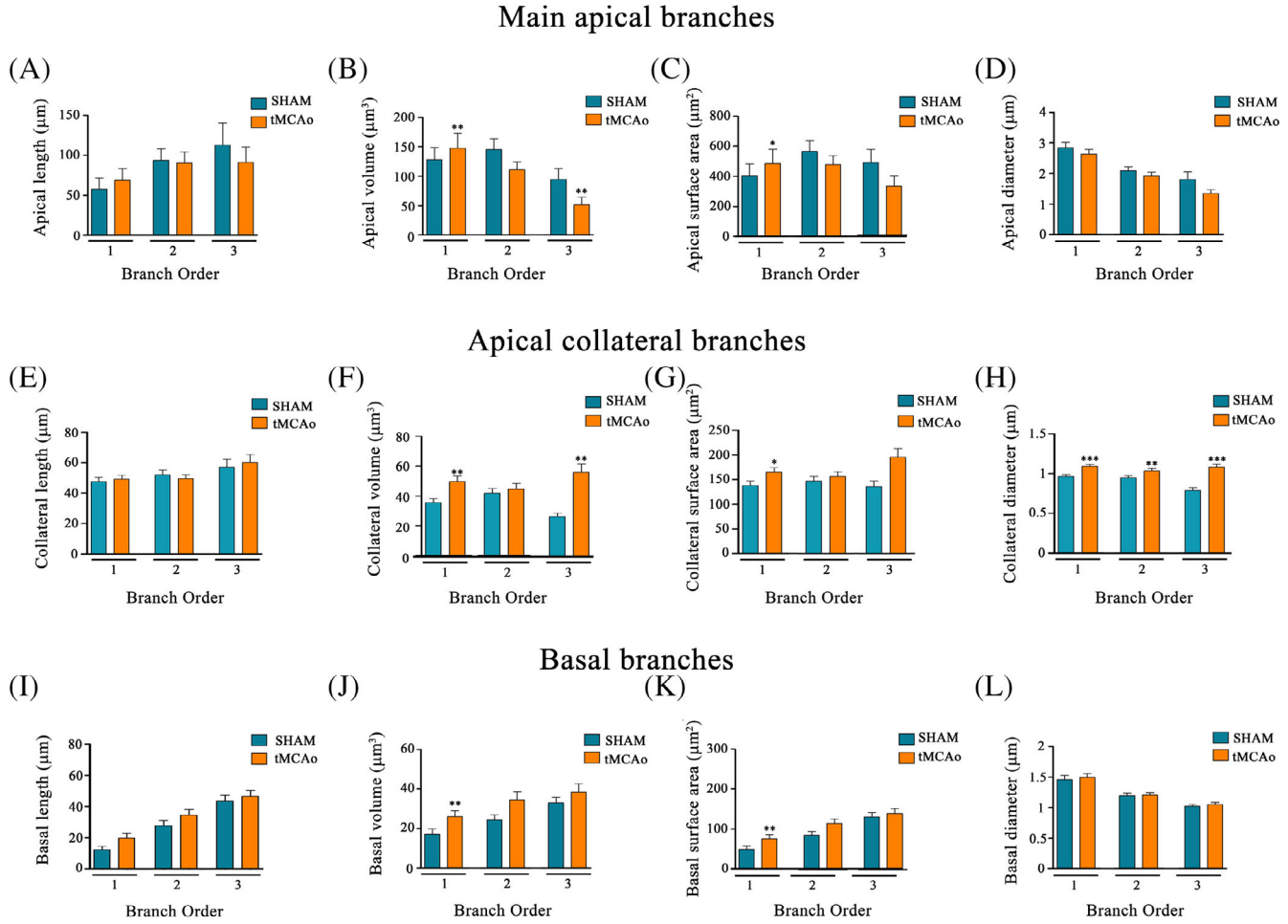

FIGURE 4 Analysis of the complexity of specific neuronal compartments. (A–D) Graphs showing the dendritic segment average (unpaired Mann–Whitney test) of several morphological parameters expressed per branch order (1, 2, and 3): (A,E,I) dendritic length, (B,F,J) dendritic volume, (C,G,K) dendritic surface area, and (D,H,L) dendritic diameter in (A–D) main apical branches, (E–H) apical collateral branches, and (I–L) basal branches. Only dendritic segments that were complete, and thus excluding incomplete endings, were included in this analysis (30 individual branches per group; $n = 4$–6 mice per group).

collateral dendritic length (unpaired Mann–Whitney, $p > 0.05$; Figure 4E).

3.2 | Pyramidal basal dendritic arbors of the contralesional CA1 field show higher neuronal complexity

The neuronal complexity in basal arbors (*stratum oriens*) was analyzed similarly to the apical dendritic arbors. The basal dendritic arbor is defined as the system of large basal dendrites that emerges laterally or downward from the base of the soma (*stratum oriens*) [34].

Significant differences were found in tMCAo compared with sham-operated mice in one or both of the statistical analyses carried out for each morphological parameter studied (see Table 1): tMCAo showed a higher dendritic length (Figure 5A,B), dendritic surface area (Figure 5E,F), and number of intersections (Figure 5I,J). Regarding dendritic volume and dendritic diameter, no significant differences were found in tMCAo compared with sham-operated mice (Figure 5C,D and Figure 5G,H, respectively).

Likewise, the same morphometric parameters were measured per branch order (1, 2, and 3) as described above (Figure 4). The basal dendritic volume was statistically higher in tMCAo mice for dendritic segment order 1 compared with sham-operated mice (Mann–Whitney, $p = 0.01$; Figure 4J). Similarly, branch order 1 showed a higher basal dendritic surface area in tMCAo (unpaired Mann–Whitney, $p = 0.01$; Figure 4K). No statistical differences were found for basal dendritic length and basal dendritic diameter in the analysis (unpaired Mann–Whitney, $p > 0.05$; Figure 4I,L, respectively).

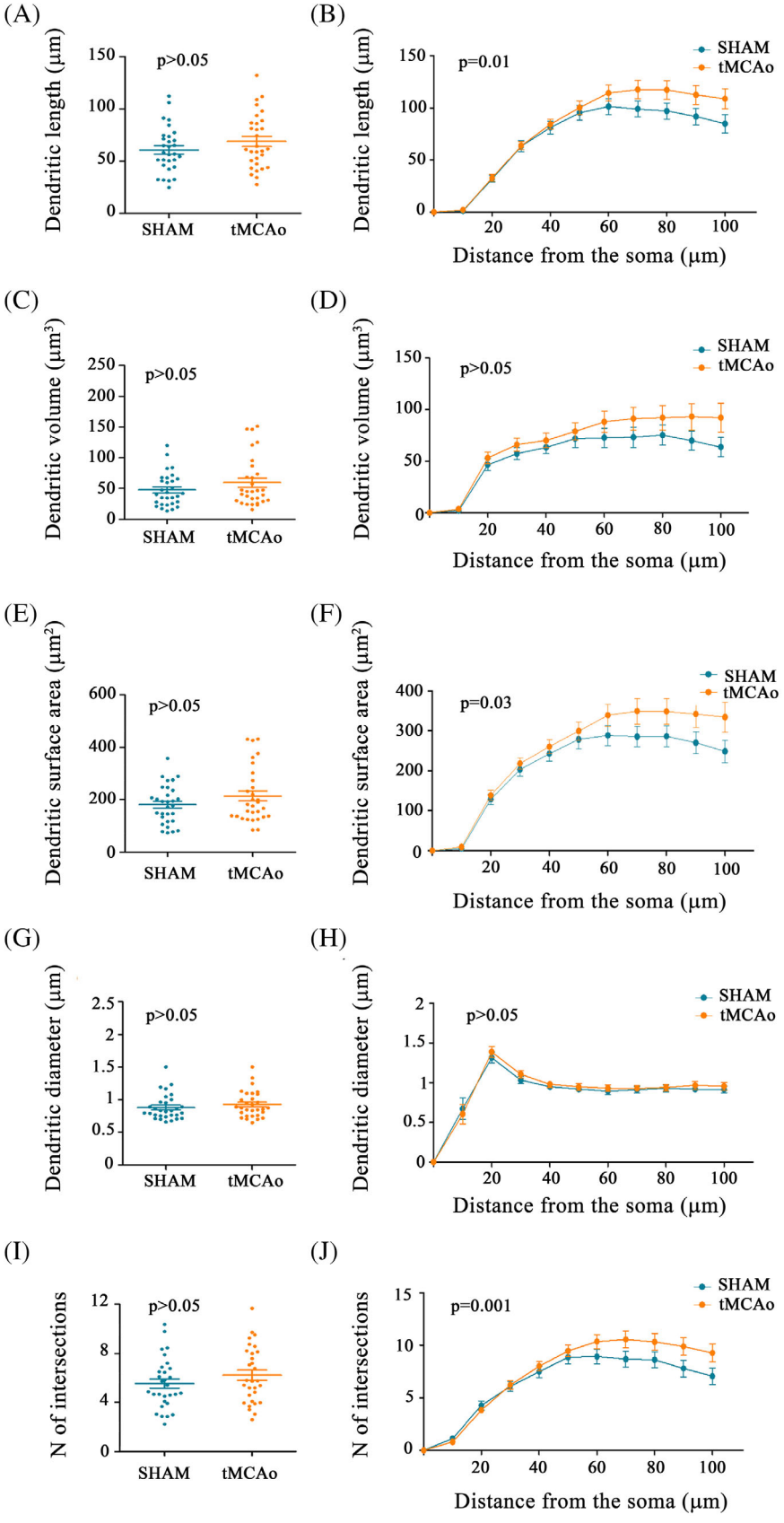

FIGURE 5 Analysis of the complexity of basal dendritic arbors. Comparative morphometric analysis (30 individual basal branches per group) between sham-operated and tMCAo mice ($n = 4$–6 mice per group) of (A,B) dendritic length, (C,D) dendritic volume, (E,F) dendritic surface area, (G,H) dendritic diameter and (I,J) number of intersections, as the average (A,C,E,G,I; unpaired Mann–Whitney test) and as a function of the distance from the soma (B,D,F,H,J; Two-way ANOVA repeated measures).

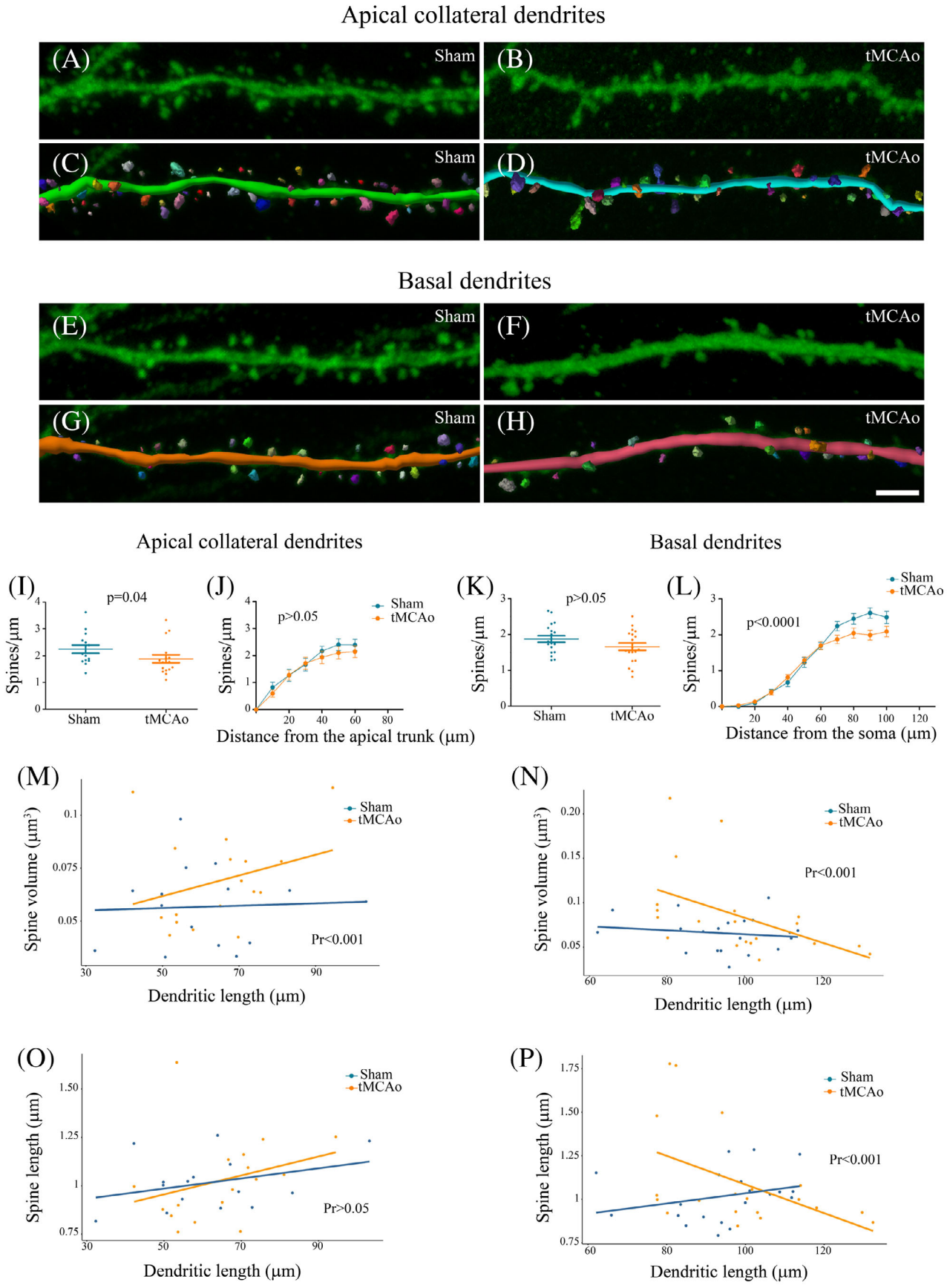

FIGURE 6 Legend on next page.

3.3 | Spines of pyramidal neurons in the contralesional CA1 field show a lower density

To test the hypothesis that ischemic stroke could induce alterations in spine density and morphology, we performed a detailed analysis of the spine microanatomy in CA1 pyramidal neurons (Figure 6), both in apical (*stratum radiatum*) and basal (*stratum oriens*) dendritic arbors in the contralesional hemisphere.

For the apical collateral dendrites, spine density was measured, assessing a total dendritic length of 1626 μm in sham-operated and 2012 μm in tMCAo mice. We found that tMCAo had a significantly lower spine density than sham mice (sham-operated 2.24 ± 0.15 spines/μm, 3704 spines; tMCAo: 1.88 ± 0.14 spines/μm, 3819 spines; Mann–Whitney test, $p = 0.04$; Figure 6I). However, no significant differences were found in spine density as a function of the distance from the soma (Two-way ANOVA, $p > 0.05$; $F = 0.69$, d.f. = 5; Figure 6J).

Spine density for basal dendrites was measured assessing a total dendritic length of 3039 μm in sham-operated and 3216 μm in tMCAo mice (sham-operated 1.87 ± 0.08 spines/μm, 5621 spines; tMCAo: 1.66 ± 0.09 spines/μm, 5387 spines; Mann–Whitney, $p = 0.16$; Figure 6K).

Significant differences were found between groups in spine density as a function of the distance from the soma (Two-way ANOVA, $p < 0.0001$; $F = 3.9$, d.f. = 9; Figure 6L).

Similarly, analyses of spine morphology were performed in the same groups of dendrites (collateral and basal dendrites).

No significant differences were found in apical collateral dendrites regarding (i) the mean spine length (sham-operated: 1.01 ± 0.03 μm; tMCAo: 1.02 ± 0.05 μm; Mann–Whitney test; $p = 0.9$) or (ii) the spine volume (sham-operated: 0.1 ± 0.04 μm^3; tMCAo: 0.1 ± 0.03 μm^3; Mann–Whitney test; $p = 0.7$) between groups (sham-operated: 0.066 ± 0.008 μm^3; tMCAo: 0.069 ± 0.005 μm^3; Mann–Whitney test; $p = 0.3$; Figure S1A,C). Likewise, no significant differences were found when the mean spine length and volume were analyzed as a function of the distance from the apical trunk (Two-way ANOVA, $p > 0.05$; $F = 1.6$, d.f. = 6 and $F = 1.02$, d.f. = 6, respectively; Figure S1B,D). Moreover, no difference was found in basal dendrites when the mean spine length (sham-operated: 1.01 ± 0.03 μm; tMCAo: 1.09 ± 0.06 μm; Mann–Whitney test; $p = 0.79$) and the mean spine volume (sham-operated: 0.06 ± 0.004 μm; tMCAo: 0.08 ± 0.01 μm; Mann–Whitney test; $p = 0.9$) were compared between tMCAo and sham-operated mice (Figure S1E,G)—or as a function of the distance from the soma (Two-way ANOVA, $p > 0.05$; $F = 1.06$, d.f. = 9; $F = 1.3$, d.f. = 9, respectively; Figure S1F,H).

Furthermore, using ANCOVA test to analyze whether the dendritic length influences spine volume and length, we found significant differences (Figure 6). Apical collateral dendrites (*stratum radiatum*) in tMCAo showed a significantly higher spine volume ($Pr = 0.000964$; Figure 6M) with no differences regarding spine length compared with sham-operated mice ($Pr = 0.88$; Figure 6O). However, in basal dendrites, significant differences were found in both spine volume ($Pr = 1.35e-05$; Figure 6N) and spine length ($Pr < 2e-16$; Figure 6P) between groups.

TABLE 2 Summary of the results obtained by comparing tMCAo versus Sham-operated groups in the analysis of the pyramidal cell morphological parameters studied in the SSCx and CA1 regions.

Dendritic structure						
SSCx	**D. length**	**D. volume**	**D. S. area**	**D. diameter**	**No. of inters**	**No. of nodes**
Apical arbor	↓	↓	↓	NS	↓	NS
Basal arbor	NS	NS	NS	NS	NS	NS
CA1						
Apical arbor	↑	↑	↑	↑	NS	ND
Basal arbor	↑	NS	↑	NS	↑	ND
Dendritic spines						
SSCx	**Spine density**		**Spine volume**		**Spine length**	
Main apical dendrites	NS		*		NS	
Collateral dendrites	NS		NS		*	
Basal dendrites	NS		*		*	
CA1						
Main apical dendrites	ND		ND		ND	
Collateral dendrites	↓		**		NS	
Basal dendrites	↓		**		**	

Note: ↓, decrease; ↑, increase; NS, no significant; ND, no data.
*Significant differences in the frequency distribution analysis.
**Significant differences influenced by the dendritic length.

FIGURE 6 Analysis of spine density and morphology. (A,B) Apical collateral (*stratum radiatum*; 15–17 dendrites per group) and (E–F) basal (*stratum oriens*; 20 dendrites per group) dendritic segments from LY-injected pyramidal neurons in CA1 from (A,E) sham-operated and (B,F) tMCAo mice ($n = 3$–4 mice per group). (C,D,G,H) The same dendritic segments as in A, B, E and F, respectively, showing the 3D spine reconstruction process. Scale bar shown in M indicates 3 μm in A–H. (I–P) Comparative morphometric analysis of the spine density and spine morphology in pyramidal neurons from the contralesional CA1 hippocampal region. Spine density analysis (spines/μm) showing (I,K) the average spine density per dendrite in apical collateral dendrites (I), and basal dendrites (K) (unpaired Mann–Whitney test); and (J,L) the spine density as a function of the distance from the soma (Two-way ANOVA repeated measures) in apical collateral dendrites (J) and basal dendrites (L). (M–P) Morphometric analysis of spine volume (M,N) and spine length (O,P) influenced by the dendritic length in apical collateral dendrites (M,O) and basal dendrites (N,P) (ANCOVA test).

4 | CONCLUSIONS

It has been extensively reported that recovery of the adult brain following a stroke depends partly on the reorganization of surviving areas adjacent to the focal lesion, with neuronal reorganization and neuronal plasticity considered key processes in this recovery [52–55].

It has been shown that areas adjacent to the focal lesion exhibit alterations in the neuronal complexity of pyramidal neurons [43, 56–58] that might compensate for the loss of function in the infarcted area, adopting new functions [58–60]. In addition, it has been demonstrated that, after stroke, remote regions connected to the infarcted area can also be affected. This process has also been described in the contralesional hemisphere and is known as transcallosal diaschisis [61]. It is thought that the main mechanism responsible for this process is the loss of excitatory inputs from the damaged cerebral hemisphere to the "intact" contralesional cerebral cortex [62]. Thus, advances in the understanding of diaschisis represent an important approach that may be useful for the development of new therapeutic targets.

In the tMCAo mouse model of ischemia, we have previously reported that acute stroke selectively induces changes in the dendritic complexity and spine morphology in remote regions connected to the infarcted area. We found that pyramidal neurons in layer III of the SSCx in the contralesional hemisphere exhibit less dendritic complexity of the apical dendritic arbor—but no changes in the basal dendritic arbor. In addition, we found differences in spine morphology in both apical and basal dendrites in the contralesional hemisphere but no changes in dendritic spine density [46]. However, in the present study, we observed higher neuronal complexity and a lower density of spines in both apical and basal arbors after stroke in CA1 pyramidal neurons in the contralesional hippocampus (Table 2). Thus, contralesional pyramidal neurons are affected differently depending on where they are located in the neocortex or hippocampus. Notably, the higher neuronal complexity in tMCAo mice was primarily observed as a function of the distance from the soma and in specific neuronal compartments, indicating a microanatomical-specific alteration of neuronal complexity.

Since neuronal complexity regulates functional capacity—influencing the biophysical properties of the neuron and the capacity of input integration—the changes found in CA1 pyramidal complexity in the present study indicate significant modifications of the functional properties of these neurons in the hippocampus. Furthermore, changes in spine density and morphology also have important functional consequences. First, the lower spine density has been suggested as a compensatory response to a loss of excitatory inputs. Regarding spine morphology, significant differences were found in volume and spine length influenced by the dendritic length. This finding is also relevant from the physiological point of view since spine morphology is directly related to spine function [63–66] and alterations in spine morphology have been extensively described in neurological disorders, suggesting that modifications in spine morphology are due to alterations of the presynaptic activity [49, 67, 68]. In this regard, recent studies propose that the spine head and the spine neck are independently-regulated compartments that influence neural capacities differently and should therefore be studied separately [69].

Finally, the specific functional significance of all these changes is unknown since it would require additional physiological experiments in the same regions where we analyzed the pyramidal cell structure. However, these morphological changes in the arbors of both apical (*stratum radiatum*) and basal (*stratum oriens*) dendrites, which are involved in multiple different circuits, obviously indicate that significant alterations of hippocampal function of the contralesional hemisphere take place after acute stroke. It is also important to emphasize that, in our experiments, the ipsilateral hippocampus was dramatically damaged and although certain morphological changes of the structure of pyramidal cells in the contralesional hippocampus were statistically significant, these changes did not affect the whole neuron. In other words, the changes are less apparent than one might expect, considering that, the ipsilateral side is extensively damaged (see Figure 1C,E) and the massive commissural system that interconnects the two sides of the hippocampal formation in rodents [70]. This probably may help in the recovery of hippocampal function, but, further anatomical and physiological studies would be necessary to better understand the modifications that occur in the "intact" contralesional brain regions and are likely to be fundamental to recover functions after stroke.

AUTHOR CONTRIBUTIONS

PMS performed intracellular injections, 3D reconstruction analysis, analyzed and interpreted the data; SPA performed 3D reconstruction analysis, analyzed and interpreted the data; FH, SVF and NP developed the tMCAo model; AK performed intracellular injections and JDF conceptualized and supervised the research; PMS and JDF wrote the manuscript with input from all authors that approved the final manuscript.

ACKNOWLEDGMENTS

We would like to thank Unidad de Tecnologías Ómicas at Instituto Cajal for its useful statistical analysis service, Carmen Álvarez, Lorena Valdés and Esther Magan Garrido for their assistance and Nick Guthrie for his excellent text editing.

FUNDING INFORMATION

This work was supported by the following entities: Network of European Funding for Neuroscience Research (ERA-NET NEURON, PCI2018-092874); PID2021-127924NB-I00 (to Javier DeFelipe) and IJCI-2016-27658 (to Paula Merino-Serrais) funded by MCIN/AEI/10.13039/501100011033; and CIBER de Enfermedades Neurodegenerativas, Instituto de Salud

Carlos III (CIBERNED, CB06/05/0066). Sergio Plaza-Alonso was awarded a research fellowship from the Spanish Ministry of Universities (contract FPU19/00007). This work was funded by the Deutsche Forschungsgemeinschaft (DFG, German Research Foundation) under Germany's Excellence Strategy within the framework of the Munich Cluster for Systems Neurology (EXC 2145 SyNergy—ID 390857198) to Nikolaus Plesnila.

CONFLICT OF INTEREST STATEMENT

The authors declare no conflicts of interest.

DATA AVAILABILITY STATEMENT

All data generated or analyzed during this study are included in this published article (and its supplementary information files). Any additional information is available from the lead upon request.

ETHICS STATEMENT

All experimental procedures were conducted in accordance with European regulations, the ethical committee of Upper Bavaria (Vet 2-15-196) and in compliance with the ARRIVE (Animal Research: Reporting In Vivo Experiments) criteria [47].

ORCID

Paula Merino-Serrais https://orcid.org/0000-0002-1842-9476

REFERENCES

1. Donnan GA, Fisher M, Macleod M, Davis SM. Stroke. Lancet. 2008;371(9624):1612–23.
2. Pinkston JB, Alekseeva N, González TE. Stroke and dementia. Neurol Res. 2009;31(8):824–31.
3. Savva GM, Stephan BCM, Alzheimer's Society Vascular Dementia Systematic Review Group. Epidemiological studies of the effect of stroke on incident dementia: a systematic review. Stroke. 2010; 41(1):e41–6.
4. Makin SDJ, Turpin S, Dennis MS, Wardlaw JM. Cognitive impairment after lacunar stroke: systematic review and meta-analysis of incidence, prevalence and comparison with other stroke subtypes. J Neurol Neurosurg Psychiatry. 2013;84(8): 893–900.
5. Lenzi GL, Frackowiak RSJ, Jones T. Cerebral oxygen metabolism and blood flow in human cerebral ischemic infarction. J Cereb Blood Flow Metab. 1982;2(3):321–35.
6. Seitz RJ, Azari NP, Knorr U, Binkofski F, Herzog H, Freund HJ. The role of diaschisis in stroke recovery. Stroke. 1999;30(9): 1844–50.
7. Witte OW, Bidmon HJ, Schiene K, Redecker C, Hagemann G. Functional differentiation of multiple perilesional zones after focal cerebral ischemia. J Cereb Blood Flow Metab. 2000;20(8):1149–65.
8. Carrera E, Tononi G. Diaschisis: past, present, future. Brain. 2014;137(9):2408–22.
9. Duering M, Righart R, Csanadi E, Jouvent E, Hervé D, Chabriat H, et al. Incident subcortical infarcts induce focal thinning in connected cortical regions. Neurology. 2012;79(20): 2025–8.
10. Silasi G, Murphy TH. Stroke and the connectome: how connectivity guides therapeutic intervention. Neuron. 2014;83(6):1354–68.
11. Buetefisch CM. Role of the Contralesional hemisphere in post-stroke recovery of upper extremity motor function. Front Neurol. 2015;6:214.
12. Butz M, Steenbuck ID, van Ooyen A. Homeostatic structural plasticity can account for topology changes following deafferentation and focal stroke. Front Neuroanat. 2014;8:115.
13. Squire LR, Zola-Morgan S. The medial temporal lobe memory system. Science. 1991;253(5026):1380–6.
14. Alvarez P, Zola-Morgan S, Squire LR. Damage limited to the hippocampal region produces long-lasting memory impairment in monkeys. J Neurosci. 1995;15(5 Pt 2):3796–807.
15. Maguire EA, Gadian DG, Johnsrude IS, Good CD, Ashburner J, Frackowiak RS, et al. Navigation-related structural change in the hippocampi of taxi drivers. Proc Natl Acad Sci U S A. 2000;97(8): 4398–403.
16. Amaral D, Lavenex P. Hippocampal Neuroanatomy. In: Morris R, Amaral D, Andersen P, Bliss T, O'Keefe J, editors. The Hippocampus Book. New York: Oxford University Press; 2007. pp. 1–832.
17. Castellanos NP, Bajo R, Cuesta P, Villacorta-Atienza JA, Paúl N, Garcia-Prieto J, et al. Alteration and reorganization of functional networks: a new perspective in brain injury study. Front Hum Neurosci. 2011;5:90.
18. Poch C, Campo P. Neocortical-hippocampal dynamics of working memory in healthy and diseased brain states based on functional connectivity. Front Hum Neurosci. 2012;6:36.
19. Finke C, Bruehl H, Düzel E, Heekeren HR, Ploner CJ. Neural correlates of short-term memory reorganization in humans with hippocampal damage. J Neurosci. 2013;33(27):11061–9.
20. Jia H, Rochefort NL, Chen X, Konnerth A. Dendritic organization of sensory input to cortical neurons in vivo. Nature. 2010; 464(7293):1307–12.
21. Luebke JI. Pyramidal neurons are not generalizable building blocks of cortical networks. Front Neuroanat. 2017;11:11. https://doi.org/10.3389/fnana.2017.00011
22. Leguey I, Benavides-Piccione R, Rojo C, Larrañaga P, Bielza C, DeFelipe J. Patterns of dendritic basal field orientation of pyramidal neurons in the rat somatosensory cortex. eNeuro. 2019;5(6): ENEURO.0142-18.2018.
23. Gidon A, Zolnik TA, Fidzinski P, Bolduan F, Papoutsi A, Poirazi P, et al. Dendritic action potentials and computation in human layer 2/3 cortical neurons. Science. 2020;367(6473):83–7.
24. Häusser M, Spruston N, Stuart GJ. Diversity and dynamics of dendritic signaling. Science. 2000;290(5492):739–44.
25. Larkum ME, Nevian T, Sandler M, Polsky A, Schiller J. Synaptic integration in tuft dendrites of layer 5 pyramidal neurons: a new unifying principle. Science. 2009;325(5941):756–60.
26. DeFelipe J. The evolution of the brain, the human nature of cortical circuits, and intellectual creativity. Front Neuroanat. 2011;5:29.
27. Eyal G, Mansvelder HD, de Kock CPJ, Segev I. Dendrites impact the encoding capabilities of the axon. J Neurosci. 2014;34(24): 8063–71.
28. Stuart GJ, Spruston N. Dendritic integration: 60 years of progress. Nat Neurosci. 2015;18(12):1713–21.
29. Tang LT, Diaz-Balzac CA, Rahman M, Ramirez-Suarez NJ, Salzberg Y, Lázaro-Peña MI, et al. TIAM-1/GEF can shape somatosensory dendrites independently of its GEF activity by regulating F-actin localization. eLife. 2019;8:e38949.
30. Bourne J, Harris KM. Do thin spines learn to be mushroom spines that remember? Curr Opin Neurobiol. 2007;17(3):381–6.
31. Spruston N. Pyramidal neurons: dendritic structure and synaptic integration. Nat Rev Neurosci. 2008;9(3):206–21.
32. Kandel ER, Dudai Y, Mayford MR. The molecular and systems biology of memory. Cell. 2014;157(1):163–86.
33. DeFelipe J. The dendritic spine story: an intriguing process of discovery. Front Neuroanat. 2015;9:14.
34. DeFelipe J, Fariñas I. The pyramidal neuron of the cerebral cortex: morphological and chemical characteristics of the synaptic inputs. Prog Neurobiol. 1992;39(6):563–607.
35. Harris KM, Kater SB. Dendritic spines: cellular specializations imparting both stability and flexibility to synaptic function. Annu Rev Neurosci. 1994;17(1):341–71.

36. Harris K, Stevens J. Dendritic spines of CA 1 pyramidal cells in the rat hippocampus: serial electron microscopy with reference to their biophysical characteristics. J Neurosci. 1989;9(8):2982–97.
37. Nusser Z, Lujan R, Laube G, Roberts JDB, Molnar E, Somogyi P. Cell type and pathway dependence of synaptic AMPA receptor number and variability in the hippocampus. Neuron. 1998;21(3):545–59.
38. Majewska A, Brown E, Ross J, Yuste R. Mechanisms of calcium decay kinetics in hippocampal spines: role of spine calcium pumps and calcium diffusion through the spine neck in biochemical compartmentalization. J Neurosci. 2000;20(5):1722–34.
39. Araya R, Jiang J, Eisenthal KB, Yuste R. The spine neck filters membrane potentials. Proc Natl Acad Sci U S A. 2006;103(47): 17961–6.
40. Koleske AJ. Molecular mechanisms of dendrite stability. Nat Rev Neurosci. 2013;14(8):536–50.
41. Biernaskie J, Corbett D. Enriched rehabilitative training promotes improved forelimb motor function and enhanced dendritic growth after focal ischemic injury. J Neurosci. 2001;21(14):5272–80.
42. Xin H, Katakowski M, Wang F, Qian JY, Liu XS, Ali MM, et al. microRNA cluster miR-17-92 cluster in exosomes enhance neuroplasticity and functional recovery after stroke in rats. Stroke. 2017; 48(3):747–53.
43. Lin YH, Liang HY, Xu K, Ni HY, Dong J, Xiao H, et al. Dissociation of nNOS from PSD-95 promotes functional recovery after cerebral ischaemia in mice through reducing excessive tonic GABA release from reactive astrocytes. J Pathol. 2018;244(2): 176–88.
44. Freund TF, Buzsáki G, Leon A, Baimbridge KG, Somogyi P. Relationship of neuronal vulnerability and calcium binding protein immunoreactivity in ischemia. Exp Brain Res. 1990;83(1): 55–66.
45. Alia C, Cangi D, Massa V, Salluzzo M, Vignozzi L, Caleo M, et al. Cell-to-cell interactions mediating functional recovery after stroke. Cell. 2021;10(11):3050.
46. Merino-Serrais P, Plaza-Alonso S, Hellal F, Valero-Freitag S, Kastanauskaite A, Muñoz A, et al. Microanatomical study of pyramidal neurons in the contralesional somatosensory cortex after experimental ischemic stroke. Cereb Cortex. 2023;33(4): 1074–89.
47. Kilkenny C, Browne WJ, Cuthill IC, Emerson M, Altman DG. Improving bioscience research reporting: the ARRIVE guidelines for reporting animal research. PLoS Biol. 2010;8(6):e1000412.
48. Lourbopoulos A, Mamrak U, Roth S, Balbi M, Shrouder J, Liesz A, et al. Inadequate food and water intake determine mortality following stroke in mice. J Cereb Blood Flow Metab. 2017; 37(6):2084–97.
49. Merino-Serrais P, Benavides-Piccione R, Blazquez-Llorca L, Kastanauskaite A, Rábano A, Avila J, et al. The influence of phospho-τ on dendritic spines of cortical pyramidal neurons in patients with Alzheimer's disease. Brain. 2013;136(Pt 6):1913–28.
50. Benavides-Piccione R, Regalado-Reyes M, Fernaud-Espinosa I, Kastanauskaite A, Tapia-González S, León-Espinosa G, et al. Differential structure of hippocampal CA1 pyramidal neurons in the human and mouse. Cereb Cortex. 2020;30(2):730–52.
51. Sholl DA. Dendritic organization in the neurons of the visual and motor cortices of the cat. J Anat. 1953;87(4):387–406.
52. Carmichael ST, Archibeque I, Luke L, Nolan T, Momiy J, Li S. Growth-associated gene expression after stroke: evidence for a growth-promoting region in peri-infarct cortex. Exp Neurol. 2005; 193(2):291–311.
53. Li S, Carmichael ST. Growth-associated gene and protein expression in the region of axonal sprouting in the aged brain after stroke. Neurobiol Dis. 2006;23(2):362–73.
54. Brown CE, Li P, Boyd JD, Delaney KR, Murphy TH. Extensive turnover of dendritic spines and vascular remodeling in cortical tissues recovering from stroke. J Neurosci. 2007;27(15):4101–9.
55. Brown CE, Boyd JD, Murphy TH. Longitudinal in vivo imaging reveals balanced and branch-specific remodeling of mature cortical pyramidal dendritic arbors after stroke. J Cereb Blood Flow Metab. 2010;30(4):783–91.
56. Zhu L, Wang L, Ju F, Khan A, Cheng X, Zhang S. Reversible recovery of neuronal structures depends on the degree of neuronal damage after global cerebral ischemia in mice. Exp Neurol. 2017; 289:1–8.
57. Xie Q, Cheng J, Pan G, Wu S, Hu Q, Jiang H, et al. Treadmill exercise ameliorates focal cerebral ischemia/reperfusion-induced neurological deficit by promoting dendritic modification and synaptic plasticity via upregulating caveolin-1/VEGF signaling pathways. Exp Neurol. 2019;313:60–78.
58. Hu J, Li C, Hua Y, Liu P, Gao B, Wang Y, et al. Constraint-induced movement therapy improves functional recovery after ischemic stroke and its impacts on synaptic plasticity in sensorimotor cortex and hippocampus. Brain Res Bull. 2020;160:8–23.
59. Dijkhuizen RM, Ren J, Mandeville JB, Wu O, Ozdag FM, Moskowitz MA, et al. Functional magnetic resonance imaging of reorganization in rat brain after stroke. Proc Natl Acad Sci. 2001; 98(22):12766–71.
60. Wei L, Erinjeri JP, Rovainen CM, Woolsey TA. Collateral growth and angiogenesis around cortical stroke. Stroke. 2001;32(9):2179–84.
61. Reggia JA. Neurocomputational models of the remote effects of focal brain damage. Med Eng Phys. 2004;26(9):711–22.
62. Ruan L, Wang Y, Chen S c, Zhao T, Huang Q, Hu Z l, et al. Metabolite changes in the ipsilateral and contralateral cerebral hemispheres in rats with middle cerebral artery occlusion. Neural Regen Res. 2017;12(6):931–7.
63. Segal M. Dendritic spines and long-term plasticity. Nat Rev Neurosci. 2005;6(4):277–84.
64. Rochefort NL, Konnerth A. Dendritic spines: from structure to in vivo function. EMBO Rep. 2012;13(8):699–708.
65. Berry KP, Nedivi E. Spine dynamics: are they all the same? Neuron. 2017;96(1):43–55.
66. Cornejo VH, Ofer N, Yuste R. Voltage compartmentalization in dendritic spines in vivo. Science. 2022;375(6576):82–6.
67. Fiala JC, Spacek J, Harris KM. Dendritic spine pathology: cause or consequence of neurological disorders? Brain Res Rev. 2002; 39(1):29–54.
68. Loera-Valencia R, Vazquez-Juarez E, Muñoz A, Gerenu G, Gómez-Galán M, Lindskog M, et al. High levels of 27-hydroxycholesterol results in synaptic plasticity alterations in the hippocampus. Sci Rep. 2021;11:3736.
69. Ofer N, Berger DR, Kasthuri N, Lichtman JW, Yuste R. Ultrastructural analysis of dendritic spine necks reveals a continuum of spine morphologies. Dev Neurobiol. 2021;81(5):746–57.
70. Mai J, Majtanik M, Paxinos G. Atlas of the human brain, 4th ed. San Diego: Academic Press/Elsevier; 2016.

SUPPORTING INFORMATION

Additional supporting information can be found online in the Supporting Information section at the end of this article.

How to cite this article: Merino-Serrais P, Plaza-Alonso S, Hellal F, Valero-Freitag S, Kastanauskaite A, Plesnila N, et al. Structural changes of CA1 pyramidal neurons after stroke in the contralesional hippocampus. Brain Pathology. 2024;34(3):e13222. https://doi.org/10.1111/bpa.13222